

Photomodification of Blood Using Low- Intensity Optical Radiation

Photomodification of Blood Using Low- Intensity Optical Radiation

By

Galina Zalesskaya
and Nalalya Mitkovskaya

**Cambridge
Scholars
Publishing**



Photomodification of Blood Using Low-Intensity Optical Radiation

By Galina Zalesskaya and Nalalya Mitkovskaya

This book first published 2020

Cambridge Scholars Publishing

Lady Stephenson Library, Newcastle upon Tyne, NE6 2PA, UK

British Library Cataloguing in Publication Data

A catalogue record for this book is available from the British Library

Copyright © 2020 by Galina Zalesskaya and Nalalya Mitkovskaya

All rights for this book reserved. No part of this book may be reproduced, stored in a retrieval system, or transmitted, in any form or by any means, electronic, mechanical, photocopying, recording or otherwise, without the prior permission of the copyright owner.

ISBN (10): 1-5275-5861-4

ISBN (13): 978-1-5275-5861-8

TABLE OF CONTENTS

List of Figures.....	viii
List of Tables.....	xx
Acknowledgements	xxi
Introduction	xxii
About the Structure of the Book.....	xxiv
Abbreviations	xxvii
Chapter One.....	1
Effect of low-intensity optical radiation on the spectral-luminescent characteristics of blood irradiated <i>in vivo</i>	
1.1 Electronic absorption spectra of whole blood, erythrocytes and plasma.....	1
1.2 Infrared absorption spectra of whole blood, erythrocytes and plasma	5
1.3 Infrared spectroscopy determination of the concentration of cephalosporin antibiotics in blood.....	10
1.4 Plasma fluorescence.....	14
1.5 Spectral manifestation of blood photomodification.....	18
1.5-1 Electronic absorption spectra of the blood, erythrocytes and plasma under UV phototherapy	18
1.5-2 Effect of the laser phototherapy at wavelengths of 632.8 nm and 780 nm on electronic absorption spectra of whole blood and erythrocytes.....	24
1.5-3 The effect of laser phototherapy at wavelengths of 632.8 nm and 780 nm on infrared absorption spectra of blood, erythrocytes and plasma	26
1.5-4 Infrared absorption spectra of blood, erythrocytes and plasma under UV phototherapy	35
1.6 Effect of the <i>in vivo</i> blood irradiation using low-intensity optical radiation on plasma fluorescence	38
1.7 References.....	44

Chapter Two	49
Photomodification of blood irradiated <i>in vivo</i> using low-intensity optical radiation	
2.1 Gas composition of venous blood under phototherapy	49
2.2 The effect of phototherapy on hemoglobin oxygen saturation.....	58
2.3 Hemoglobin-oxygen affinity and oxygen capacity of blood under the phototherapy	62
2.4 The effect of phototherapy on erythrocytes of blood.....	71
2.4-1 Changes in the shape of red blood cells under the phototherapy	71
2.4-2 The electrophoretic mobility of erythrocytes under UVBI and magnetic therapy	76
2.4-3 The effect of phototherapy on the erythrocyte metabolism.....	78
2.5. The individualization of therapeutic doses of optical radiation according to blood oxygenation	82
2.6 Photomodification of blood aggregation characteristics under phototherapy.....	85
2.7 The phototherapy effect on glucose and lactate concentrations.....	92
2.8 The correction of lipid metabolism by phototherapy	97
2.8-1 The effect of UV blood irradiation on lipid metabolism.....	97
2.8-2 The effect of overvein blood irradiation on lipid metabolism	107
2.9 References.....	110
Chapter Three	114
Molecular mechanisms of the phototherapy action	
3.1 Primary photoacceptors and primary photoreactions (literature data).....	114
3.2 Interaction of optical radiation with human tissues under the phototherapy	119
3.2-1 Optical characteristics of blood and skin tissues, and the penetration depth of optical radiation.....	119
3.2-2 Blood photomodification by optical radiation at various wavelengths	127
3.2-3 The heating of human tissue during phototherapy: computer simulation	134
3.2-4 The thermal effects of overvein blood irradiation with intense infrared laser radiation.....	144
3.2-5 Modeling of laser irradiation conditions for mucosal tissues in an antimicrobial photodynamic therapy	148
3.3 The effect of magnetic therapy on blood molecules	156

3.4 The molecular mechanism of the phototherapy action based on the absorption of optical radiation by hemoglobin	162
3.5 The role of the reactive oxygen species in the therapeutic action of low-intensity optical radiation	165
3.5-1 Destruction of human tissue biomolecules initiated by reactive oxygen species	165
3.5-2 Positive effects of reactive oxygen species during the phototherapy	166
3.6 References.....	171
Chapter Four	180
The combined action of gamma radiation and low-intensity laser radiation on experimental animals (rats)	
4.1 The radioprotective action of laser radiation (literature data).....	180
4.2 The combined effect of gamma and low-intensity laser radiation on peripheral blood of rats: pre- and post- gamma exposure of blood	186
4.2-1 Goal of studies; materials and methods.....	186
4.2-2 Electronic absorption spectra of blood at combined irradiation	189
4.2-3 The effect of gamma radiation on leucocyte (WBC), lymphocyte (LYM) and granulocyte (GRA) in peripheral blood.....	192
4.2-4 The effect of gamma radiation on erythrocyte (RBC) and hemoglobin concentrations, hematocrit (Hct) values.....	195
4.2-5 The effect of gamma radiation on platelet (PLT) concentration	197
4.2-6 The effect of gamma radiation on activity of antioxidant enzymes	199
4.2-7 Changes of the mean-group number of cells and mean-group activity of SOD and CAT initiated by combined (γ +laser) and (laser+ γ) irradiation.....	200
4.2-8 The effect of gamma and combined irradiation on the individual number of cells	202
4.2-9 The effect of the laser energy density on the post-radiation number of cells and SOD activity.....	205
4.3 Possible mechanisms of the radioprotective action of low-intensity optical radiation (laser/LED).....	207
4.4 References.....	211
Conclusions	215

LIST OF FIGURES

Fig. 1-1 Absorption spectra: whole blood (A1) and erythrocytes (A2); whole blood with a higher content of oxyhemoglobin (B2) and with a lower one (B1); plasma (C).....	2
Fig. 1-2 Variation of the shape of the absorption bands at 541 and 577 nm with increase in the content of oxyhemoglobin ($F(\text{HbO}_2)$).....	3
Fig. 1-3 Infrared absorption spectra of whole blood (A) and plasma (B).....	6
Fig. 1-4 Deconvolution spectra of the infrared absorption bands of erythrocytes: (A) in range of Amide A; (B) in the ranges of Amide I and Amide II ($\Delta\nu_{1/2}=100\text{ cm}^{-1}$ (A), 30 cm^{-1} (B) and $k_{\text{enh.}}=2.5$).....	7
Fig. 1-5 Infrared absorption spectra of films: (1) prepared from an aqueous solution of ceftriaxone (concentration $c=10\text{ mg/mL}$, dark line) and (2) from whole blood (film thickness $d=5\text{ }\mu\text{m}$, light line).....	11
Fig. 1-6 Ratio of optical densities $D_{\text{bl}}/D_{\text{cefr}}$ (the blood bands at $\nu_{\text{max}}=1654$ (1), 1540 (2), 1402 cm^{-1} (3) and ceftriaxone band at $\nu_{\text{max}}=1764\text{ cm}^{-1}$) vs. ceftriaxone concentration ($r=0.98$, $p<0.05$ (1); $r=0.99$, $p<0.05$ (2, 3)).....	13
Fig. 1-7 (A) Plasma fluorescence spectra ($\lambda_{\text{ex}}=280\text{ nm}$): a healthy person (1) and a CVD patient (2); excitation spectrum (3); (B) deconvolution spectra of the plasma fluorescence of a healthy person (1), the CVD patient (2) ($\Delta\nu_{1/2}=40\text{ nm}$ and $k_{\text{enh.}}=2.5$) [36].....	16
Fig. 1-8 UVBI effect on the plasma absorption spectra of 2 patients: solid line – before UVBI; dotted line – after 5 UVBI procedures.....	21
Fig. 1-9 Electronic absorption spectra of the blood samples: (1) before UVBI and (2) after 5 UVBI procedures with $E=0.06\text{ J/cm}^2$; (A) the Soret bands normalized by intensity at the band maximum; (B) doublet of bands at 541 and 577 nm.....	22
Fig. 1-10 (A) Electronic absorption spectra of erythrocytes: before UVBI (1) and after 5 UVBI procedures (2); (B) the Soret bands normalized by intensity at the band maximum; (C) doublet of bands at 541 and 577 nm (the notation as before).....	22
Fig. 1-11 The Soret bands in the blood absorption spectra of two CVD patients before UVBI (A1; B1), during the UVBI procedure (A2) and after the end of the UVBI course (B2). The corresponding	

- deconvolution spectra before UVBI (C1; D1), during the UVBI procedure (C2), after the end of the UVBI course (D2)..... 23
- Fig. 1-12 (A) Electronic absorption spectra of blood: before irradiation (1) and one hour after the end of 8 OVBI procedures (2); (B) the Soret bands normalized by intensity at the band maximum; (C) doublet of the bands at 541 and 577 nm ($\lambda_{ir}=780$ nm, the laser power 10 mW, the magnetic field strength 35 mT, the irradiation time $t=15$ min). Designations (1) and (2) are the same as in A..... 25
- Fig. 1-13 Infrared absorption spectra of blood before IVBI (solid line) and after the end of the course (dotted line). ($\lambda_{ir}=670$ nm, the exposure time $t=20$ min, 2 mW at the output of the light guide)..... 26
- Fig. 1-14 Deconvolution spectra of infrared absorption bands of whole blood: (A) Amide I and Amide II ranges; (B) Amide III range (before IVBI (1) and after 8 IVBI procedures (2) ($\Delta\nu_{1/2}=30$ cm⁻¹ (A), $\Delta\nu_{1/2}=35$ cm⁻¹ (B) and $k_{enh.}=2.5$))...... 27
- Fig. 1-15 Deconvolution spectra of the infrared absorption band of the NH stretching vibrations (whole blood samples): (1) before OVBI; (2) after OVBI ($\lambda_{ir}=670$ nm)..... 28
- Fig. 1-16 Infrared spectra of plasma samples prepared from blood taken before irradiation (solid line) and after the end of the IVBI course (dotted line) ($\lambda_{ir}=632.8$ nm)..... 28
- Fig. 1-17 Deconvolution spectra of infrared absorption bands of erythrocytes for 2 patients in the Amide I and II ranges: (A) increasing and (B) decreasing the content of oxyhemoglobin: before OVBI (1) and after OVBI (2) ($\lambda_{ir}=670$ nm)..... 29
- Fig. 1-18 Deconvolution spectra of the infrared bands of blood in the Amide III range (normalized by the intensity at the maximum of the band at $\nu_{max}=1232.5$ cm⁻¹). (A) Increasing and (B) decreasing the content of oxyhemoglobin: before OVBI (1) and after OVBI (2) at $\lambda_{ir}=670$ nm 30
- Fig. 1-19 Infrared absorption spectra of blood (A) and deconvolution spectra (B) in the range of the band of stretching vibrations of phosphate groups: before IVBI (1), after 8 IVBI procedures (2) ($\Delta\nu_{1/2}=30$ cm⁻¹, $k_{enh.}=2.5$)..... 34
- Fig. 1-20 Infrared absorption spectra of erythrocytes: before (solid line) and after 5 UVBI procedures with $E=0.07$ J/cm² (dotted line) 35
- Fig. 1-21 Deconvolution spectra of the infrared absorption bands of erythrocytes: (A) the Amid A range (normalized by intensity at the maximum of the band at 3300 cm⁻¹); (B) the Amide I and Amide II ranges (normalized by intensity at the maximum of the band at 1655 cm⁻¹): solid curve – before UVBI, dashed curve – after 5 UVBI

procedures with $E = 0.07 \text{ J/cm}^2$ ($\Delta\nu_{1/2} = 100 \text{ cm}^{-1}$ (A) and $\Delta\nu_{1/2} = 30 \text{ cm}^{-1}$ (B), $k_{\text{enh.}} = 2.5$).....	36
Fig. 1-22 Deconvolution spectra of the infrared absorption bands of plasma: (A) the Amide A range ($\Delta\nu_{1/2} = 100 \text{ cm}^{-1}$, $k_{\text{enh.}} = 2.5$); (B) Amide I and Amide II ranges ($\Delta\nu_{1/2} = 30 \text{ cm}^{-1}$, $k_{\text{enh.}} = 2.5$), solid line – before UVBI, dotted line – after 5 UVBI procedures with $E = 0.07 \text{ J/cm}^2$	36
Fig. 1-23 Infrared deconvolution spectra of the blood absorption bands in the Amide III range (normalized by the intensity at the maximum of the band at 1306 cm^{-1}): before (1) and after UVBI (2), ($\Delta\nu_{1/2} = 30 \text{ cm}^{-1}$, $k_{\text{enh.}} = 2.5$); (A) the decrease and (B) the increase of the oxyhemoglobin content.....	37
Fig. 1-24 (A-C) Plasma fluorescence spectra of 3 CVD patients: before (1) and after the UVBI course (2); (A'–C') the corresponding deconvolution spectra ($\Delta\lambda_{1/2} = 40 \text{ nm}$, $k_{\text{enh.}} = 2.5$) ($\lambda_{\text{ex}} = 280 \text{ nm}$).....	39
Fig. 1-25 Plasma fluorescence spectra of 2 patients: (A1) before IVBI ($\lambda_{\text{ir.}} = 670 \text{ nm}$, 3mW , the exposure time $t = 15 \text{ min}$); (B1) before OVBI ($\lambda_{\text{ex.}} = 670\text{nm}$, 10mW , the exposure time $t = 15 \text{ min}$), (A2) after 5 IVBI procedures and (B2) after 5 OVBI procedures; (A', B') – corresponding deconvolution spectra ($\Delta\lambda_{1/2} = 35 \text{ nm}$, $k_{\text{enh.}} = 2.5$)	40
Fig. 1-26 Maxima position (λ_{max}) of the plasma fluorescence spectra vs. pH values: ●— before UVBI, ○— after UVBI ($r = 0.7$, $p < 0.05$)	43
Fig. 2-1 Changes in the gas partial pressures in venous blood of one of the patients during the IVBI course ($\lambda = 670 \text{ nm}$): (1) p_{vO_2} before the procedure (□) and during the procedure (■); (2) p_{vCO_2} before the procedure (○) and during the procedure (●).....	51
Fig. 2-2 Changes in the oxygen partial pressure p_{vO_2} in venous blood of one of the patients: (A) during and after UVBI and (B) during and after OVBI procedure ($\lambda_{\text{ir.}} = 670 \text{ nm}$).....	51
Fig. 2-3 Photoinduced changes in the oxygen partial pressure (Δp_{vO_2}) and the carbon dioxide partial pressure (Δp_{vCO_2}) vs. ΔS_{vO_2} under UVBI ($r = 0.81$, $p < 0.001$ (A), and $r = -0.8$, $p < 0.004$ (B)). Each point reflects the changes of the gas pressures in blood of one patient	52
Fig 2-4 Photoinduced changes in the oxygen partial pressure (Δp_{vO_2}) and the carbon dioxide partial pressure (Δp_{vCO_2}) vs. ΔS_{vO_2} under OVBI ($r = 0.81$, $p < 0.001$ (A), and $r = -0.70$, $p < 0.004$ (B)). Each point reflects the changes of the gas partial pressures in blood of one patient	53
Fig. 2-5 (A) The oxygen partial pressure p_{vO_2} in venous blood during the UVBI course. (B) The changes in the growth of p_{vO_2} (Δp_{vO_2}) during the IVBI course. For both UVBI and IVBI, the results belong to one patient	54

- Fig. 2-6 Changes of the carbon dioxide partial pressure (Δp_{vCO_2}) initiated by UVBI vs. the initial values of p_{vCO_2} in venous blood ($r = -0.61$, $p < 0.01$). Each point reflects the changes in blood of one patient 55
- Fig. 2-7 Normalizing UVBI effect on the mean-group partial pressures p_{vCO_2} in patient's blood of the two subgroups with different initial values of p_{vCO_2} and, as a consequence, with a different direction of p_{vCO_2} changes in these groups after 5 UVBI procedures 56
- Fig. 2-8 (A) Photoinduced changes in the bicarbonate ion concentration ($\Delta C_{\text{HCO}_3^-}$) vs. ΔS_{vO_2} . (B) Changes in pH value (ΔpH) vs. ΔS_{vO_2} in venous blood under UVBI. (A) $r = -0.64$, $p < 0.002$; (B) $r = 0.52$, $p < 0.02$). Each point in Figs 2-8 reflects the changes in blood of one patient 56
- Fig. 2-9 Photoinduced changes in the bicarbonate ion concentrations ($\Delta C_{\text{HCO}_3^-}$) vs. initial values ($C_{\text{HCO}_3^-}$) in venous blood: (A) under UVBI ($r = -0.7$, $p < 0.0012$) and (B) under OVBI ($r = -0.66$, $p < 0.0015$). Each point in Figs 2-9 reflects the changes of the bicarbonate ion (HCO_3^-) concentration in blood of one patient..... 57
- Fig. 2-10 Normalizing effect of 5 UVBI procedures on the mean-group concentrations of bicarbonate ion in blood of the patients of two subgroups with different initial concentrations..... 57
- Fig. 2-11 Changes of the degree of hemoglobin oxygen saturation in venous blood (ΔS_{vO_2}) after the end of PT course vs. initial S_{vO_2} values: (A) after UVBI and (B) after OVBI. Each point corresponds to the results obtained for one patient 60
- Fig. 2-12 Changes in the degree of hemoglobin oxygen saturation S_{vO_2} in venous blood of one of the patients during the OVBI course: (O) –before the procedure, (□) –during the procedure. The numbers indicate the procedure number..... 61
- Fig. 2-13 The degree of hemoglobin oxygen saturation (S_{vO_2}) in venous blood vs. the procedure number. The S_{vO_2} values are measured after the end of procedures: (1) IVBI and (2) UVBI. Each point reflects the value of S_{vO_2} in venous blood of one patient..... 61
- Fig. 2-14 AVDO₂ changes vs. ΔS_{vO_2} after the OVBI course (A) and after the UVBI course (B). Each point in the Figs corresponds to the data for one patient. (A) $r = -0.97$ $p < 0.001$; (B) $r = -0.95$ $p < 0.001$ 66
- Fig. 2-15 Oxyhemoglobin dissociation curves (ODC) before UVBI (1, 2) and after UVBI (3, 4) for the CVD patients with different initial blood oxygenation. Patient 1 (ODC-1, 3): before UVBI $-p_{\text{vO}_2} = 19.8$ mm Hg, $S_{\text{vO}_2} = 32.3\%$; after UVBI $-p_{\text{vO}_2} = 24.1$ mm Hg, $S_{\text{vO}_2} = 44.2\%$; patient 2 (ODC-2, 4): before UVBI $-p_{\text{vO}_2} = 26.5$ mm Hg, $S_{\text{vO}_2} = 39.1\%$; after UVBI $-p_{\text{vO}_2} = 20.2$ mm Hg, $S_{\text{vO}_2} = 30.9\%$ 68

- Fig. 2-16 The p50 changes ($\Delta p50$) vs. the initial p50 value in venous blood of individual patients: (A) after UVBI and (B) after OVBI courses. (A) $r = -0.68$ $p < 0.001$; (B) $r = -0.72$ $p < 0.001$ 68
- Fig. 2-17 Photoinduced p50 changes ($\Delta p50$) vs. ΔS_vO_2 after the UVBI course (A) ($r = 0.64$, $p < 0.006$) and (B) after the OVBI course ($r = 0.55$, $p < 0.013$). Each point corresponds to the result for one patient..... 69
- Fig. 2-18 The RBC volume changes during IVBI procedures. The values denoted by (★) are obtained during the procedure 73
- Fig. 2-19 Electrophoretic mobility of erythrocytes in the CVD patients... 77
- Fig. 2-20 Changes during the UVBI course: Hct in blood samples of patients with different initial Hct values (1, 2); K^+ ion concentration (3), and Na^+ ion concentration (4) in blood samples of patient number 1 79
- Fig. 2-21 Changes during the UVBI course: Hb concentration (C_{Hb}) in blood samples of patients with high initial C_{Hb} (1) and with normal C_{Hb} (2); the oxygen partial pressure p_vO_2 (3) for patient 1 79
- Fig. 2-22 Changes during the IVBI course: (1) Hb concentration, (2) oxyhemoglobin content, and (3) K^+ ion concentration in blood of one of the patients 80
- Fig. 2-23 Changes in hemoglobin concentration (ΔC_{Hb}) vs. the initial C_{Hb} value after the UVBI (●) and after OVBI (□) courses, $r = -0.7$, $p < 0.001$). Each point corresponds to the data for one patient..... 81
- Fig. 2-24 Changes of hemoglobin oxygen saturation in venous blood (S_vO_2) during PT courses. (1) The UVBI course: before the procedure (●), (○) during procedure in blood samples taken from UV cuvette; (2) before the UVBI procedure (▲), in blood samples taken during the procedure (△); (3) the OVBI course: before procedure (■), during the procedure (□) 82
- Fig. 2-25 (1, 2) The changes of oxygen utilization rate ($R_{util.}$) in two patients during the UVBI course; (3) oxygen partial pressure in venous blood (p_vO_2) in patient 1 and (4) in patient 2..... 83
- Fig. 2-26 Relative mean-group blood viscosity η_{bl}/η_w before and after the UVBI course 86
- Fig. 2-27 Relative mean-group plasma viscosity η_{pl}/η_w . before and after the UVBI course 86
- Fig. 2-28 Changes, initiated by UVBI in the blood viscosity ($\Delta\eta_{bl}$). ($r = -0.63$ at $p < 0.04$) and the plasma viscosity ($\Delta\eta_{pl}$). ($r = -0.75$ at $p < 0.01$) vs. their initial values in individual patients..... 87
- Fig. 2-29 Changes in aPTT ($\Delta aPTT$), TC (ΔTC) and PT ratio (ΔPT_{ratio}) initiated by UVBI vs. their initial values ($r = -0.64$, $p < 0.002$ for aPTT; $r = -0.8$, $p < 0.001$ for TCT; $r = -0.57$, $p < 0.02$ for PT ratio)..... 88

- Fig. 2-30 Regulatory effect of 5 UVBI procedures on the mean aPTT values for two subgroups of patients having different initial values.... 89
- Fig. 2-31 Changes in aPTT (Δ_{aPTT}) initiated by OVBI vs. aPTT values in individual patients ($r = -0.64$, $p < 0.002$)..... 90
- Fig. 2-32 Changes in TC (Δ_{TC}) initiated by OVBI vs. TC initial values in individual patients ($r = -0.8$, $p < 0.001$) 90
- Fig. 2-33 OVBI initiated changes in PT ratio ($\Delta_{PT \text{ ratio}}$) vs. PT ratio initial values in individual patients ($r = -0.78$, $p < 0.002$) 90
- Fig. 2-34 OVBI initiated changes in INR (Δ_{INR}) vs. INR initial values in individual patients ($r = -0.72$, $p < 0.001$) 90
- Fig. 2-35 Changes of TCT and aPTT under UVBI (●) and OVBI (□): (A) Δ_{TCT} vs. ΔS_{VO_2} ; (B) aPTT (Δ_{aPTT}) vs. ΔS_{VO_2} 91
- Fig. 2-36 Oscillations during the IVBI course ($\lambda_{ir} = 670 \text{ nm}$): (1) oxygen partial pressure p_{VO_2} (before the procedure (□), during the procedure (■)), (2) lactate concentration C_{lac} . (before IVBI (○), during the IVBI procedure (●)) 93
- Fig. 2-37 Changes initiated by UVBI in the glucose and lactate concentrations: (A) ΔC_{gl} vs. C_{gl} ; (C) ΔC_{lac} vs. C_{lac} ; (B, D) ΔC_{gl} and ΔC_{lac} vs. the S_{VO_2} photoinduced changes (ΔS_{VO_2}) ($r = -0.75$ for $p < 0.0001$ (A) and $r = -0.62$ for $p < 0.001$ (C))..... 94
- Fig. 2-38 (A) Changes initiated by OVBI (●) and UVBI (□) in the glucose (ΔC_{gl}) and lactate (ΔC_{lac}) concentrations: (A) ΔC_{gl} vs. C_{gl} ; ΔC_{lac} vs. C_{lac} ; (B) ΔC_{gl} and ΔC_{lac} vs. ΔS_{VO_2} — the photoinduced changes in S_{VO_2} ($r = -0.58$ for $p < 0.01$ (ΔC_{gl}) and $r = -0.41$ for $p < 0.06$ (ΔC_{lac})). Each point corresponds to the data for one patient 95
- Fig. 2-39 Concentration changes initiated by UVBI in cholesterol fraction in the different patients: (A) ΔC_C vs. C_C ($r = -0.69$, $p < 0.01$), (B) ΔC_{LDL-C} vs. C_{LDL-C} ($r = -0.70$, $p < 0.01$), (C) ΔC_{HDL-C} vs. C_{HDL-C} ($r = 0.82$, $p < 0.01$), (D) ΔC_{TG} vs. C_{TG} ($r = -0.58$, $p < 0.01$). Each point in Fig. 2-39 corresponds to the data for one patient 98
- Fig. 2-40 Changes initiated by UVBI in the concentrations of total cholesterol (C_C) and low density lipoprotein cholesterol (C_{LDL-C}) in patients with the different degree of hemoglobin oxygen saturation: (A) ΔC_{TC} vs. ΔS_{VO_2} ; (B) ΔC_{LDL-C} vs. ΔS_{VO_2} . Each point in Fig. 2-40 corresponds to the data for one patient 100
- Fig. 2-41 UVBI-initiated change in infrared plasma absorption bands in the range of symmetric CH-stretching vibrations for 2 patients: (A) the cholesterol concentration in the first patient was $C_C = 4.8 \text{ mmol/L}$ before UVBI (curve 1) and 4.1 mmol/L after UVBI (curve 2); (B) in

the second patient – $C_C = 7.9$ mmol/L before UVBI (curve 1) and 5.9 mmol/L after UVBI (curve 2)	101
Fig. 2-42 Deconvolution spectra of infrared plasma absorption bands in the ranges of Amide I and Amide II: the patient with $C_C = 7.9$ mmol/L before UVBI (solid line) and 5.9 mmol/L after UVBI (dotted line) ..	101
Fig. 2-43 Normalizing effect of 5 UVBI procedures on cholesterol concentration in two patient subgroups which differ the initial cholesterol concentrations and, as a consequence, the direction of changes in cholesterol concentration (C_C) after the UVBI course (■ – concentration decrease, ● – concentration increase)	103
Fig. 2-44 Changes of relative erythrocyte concentrations ($\Delta C_{RBC}/C_{RBC}$) under UVBI in patients with different cholesterol concentrations: $\Delta C_{RBC}/C_{RBC}$ vs. $\Delta C_C/C_C$	106
Fig. 2-45 Effect of the initial C_C and C_{C-LDL} concentrations in blood of the individual patients on the change in their concentrations initiated by OVBI ($r = -0.70$, $p < 0.01$ for ΔC_C vs. C_C and $r = -0.58$, $p < 0.01$ for ΔC_{LDL-C} vs. C_{LDL-C})	108
Fig. 2-46 The OVBI effect on mean-group lipid concentrations in a group of CVD patients ($n=25$). Before the course: (1) C, (3) LDL-C, (5) HDL-C, (7) TG and after the course end – (2), (4), (6), (8) respectively	108
Fig. 2-47 Changes in LDL-C concentration (ΔC_{LDL-C}) in individual patients vs. ΔS_vO_2 -photoinduced changes in the degree of hemoglobin oxygen saturation in venous blood (ΔS_vO_2)	109
Fig. 3-1 Absorption spectra: (1) blood (hematocrit (Ht)-44%), (2) water [24]. Phosphate buffer: pH = 7.4; 0.3 mol/L	120
Fig. 3-2 Spectral dependences of the scattering coefficient μ_s and the anisotropy factor g for blood [26]. Phosphate buffer: pH = 7.4; 0.3 mol/L	120
Fig. 3-3 Spectral dependences of the skin coefficients: absorption – μ_a and scattering – μ_{s_s} , measured <i>in vivo</i> [33]	122
Fig. 3-4 (A) The blood transmission vs. z – the light penetration depth for different wavelengths: (1) $\lambda=524$ nm; (2) $\lambda=630$ nm; (3) $\lambda=905$ nm); skin tissue transmission: (4) $\lambda=524$ nm; (5) $\lambda=630$ nm; (6) $\lambda=890$ nm. (B) The transmission spectrum of skin tissues at depths of 1 and 2 mm	123
Fig. 3-5 A volume distribution of the intensity of the optical radiation sources in a vein of cylindrical form in the plane of section, which is normal to the axis of the cylinder	124
Fig. 3-6(A)The depth of light penetration into blood and (B) into the skin tissue vs. wavelength of optical radiation: (1) the reduced scattering	

- coefficient; (2) the spectrum of the effective penetration depth; (3) the spectrum of full penetration depth 125
- Fig. 3-7 The $\mu_a(\lambda)/\mu_{\text{ef}}(\lambda)$ ratio as a function of wavelength. The effective spectral absorption coefficients of blood ($C_{\text{ef}}(\lambda, z)$) are shown by vertical bars..... 129
- Fig. 3-8 The dependence of the OVBI induced changes on the initial degree of the hemoglobin oxygen saturation $S_V\text{O}_2$ (curve 2 of each panel): (A) oxyHb content ($r = -0.89$, $p < 0.001$); (B) glucose concentration ($r = -0.54$, $p < 0.001$); (C) the concentration of cholesterol ($r = -0.67$, $p < 0.001$). Curves 1 of each panel show the dependence of the blood absorption coefficient μ_a on $S_V\text{O}_2$ 132
- Fig. 3-9 Regulatory effects of 7 OVBI procedures: (A) the degree of hemoglobin oxygen saturation $S_V\text{O}_2$; (B) the cholesterol concentration C_C : (●) for the patients of the subgroup with values higher than median value; (■) for the patients of the subgroup with values lower than median value..... 133
- Fig. 3-10 (A) The temperature of the tissue heating (T) under OVBI as a function of the irradiation time t: (1) blood in the blood vessel ($\lambda_{\text{ir}} = 780$ nm, $I_0 = 0.02$ W/cm²); (2) on the front wall of the vessel; (3) on the skin surface; (B) heating temperature T vs. the tissue penetration depth z: (1) $\lambda_{\text{ir}} = 470$ nm, $I_0 = 0.035$ W/cm²; (2) $\lambda_{\text{ir}} = 670$ nm, $I_0 = 0.25$ W/cm²; (3) $\lambda_{\text{ir}} = 780$ nm, $I_0 = 0.01$ W/cm²)..... 141
- Fig. 3-11 A volume temperature distribution under OVBI ($\lambda_{\text{ir}} = 780$ nm, 0.004 W/cm², $t = 10$ min) in a vein $d = 3$ mm. The arrow indicates the direction of the radiation propagation..... 142
- Fig. 3-12 The temperature of tissue heating under OVBI ($\lambda_{\text{ir}} = 670$ nm, $I_0 = 0.25$ W/cm²) vs. the irradiation time t: (1) on the skin surface; (2) on the front wall of the vessel; (3) blood in the blood vessel..... 144
- Fig. 3-13 The temperature of tissue heating under OVBI ($\lambda_{\text{ir}} = 470$ nm, $I_0 = 0.035$ W/cm²) vs. irradiation time t: (1) on the skin surface; (2) on the front wall of the vessel; (3) blood in the blood vessel 144
- Fig. 3-14 (A) Deconvolution spectra of the Soret bands ($\Delta\lambda_{1/2} = 50$ nm and $k_{\text{enh}} = 2.5$) of blood samples: (1) intact rats; (2) samples taken on the second (3) and on the 5th day after OVBI. (B) Absorption spectra of blood samples in the range of 600–1000 nm: (1) intact rats, samples taken on the 2nd (2) and (3) on the 5th day after OVBI 145
- Fig. 3-15 Temperature of tissue heating (T) under OVBI ($\lambda_{\text{ir}} = 2000$ nm) vs. irradiation time t: (A) on the skin surface (dotted line) and in the blood vessel (solid lines); (B) temperature variation over depth of the tissue z. Radiation power densities: 1 W/cm² (1), 2 W/cm² (2), and 6.4 W/cm² (3)..... 148

- Fig. 3-16 Distribution of the MB concentration over the depth of the mucosal tissue for tissue staining time $t_{\text{stain}} = 1$ (1), 2.5 (2), 5 (3) and 10 (4) minutes. (5) Relative sensitizer amount S_{rel} diffusing into a layer $d=500 \mu\text{m}$ of mucosal tissue vs. staining time 151
- Fig. 3-17 Distribution of laser energy, absorbed per unit volume of scattering tissue in the direction of propagation of the laser radiation ($Q, \text{W}/\text{cm}^3$), $\lambda_{\text{ir.}} = 670 \text{ nm}$, $I = 0.09 \text{ W}/\text{cm}^2$. (A) (1) without the dye and (2) for thickness of the stained layer $d = 50 \mu\text{m}$, $C(t)_{\text{rel}} = 0.32$, $t_{\text{stain}} = 10 \text{ min}$, $\mu_{\text{PS}} = 4.5 \text{ cm}^{-1}$. (B) (1) without the dye; (2) for thickness of the stained layer $d = 500 \mu\text{m}$, $C(t)_{\text{rel}} = 0.43$, $t_{\text{stain}} = 2.5 \text{ min}$, $\mu_{\text{PS}} = 25.9 \text{ cm}^{-1}$; (3) $C(t)_{\text{rel}} = 0.56$, $t_{\text{stain}} = 5 \text{ min}$, $\mu_{\text{PS}} = 34.0 \text{ cm}^{-1}$; (4) $C(t)_{\text{rel}} = 0.715$, $t_{\text{stain}} = 10 \text{ min}$, $\mu_{\text{PS}} = 43.0 \text{ cm}^{-1}$ 152
- Fig. 3-18 Distribution of laser energy absorbed per unit volume of scattering tissue in the direction of the radiation propagation ($Q, \text{W}/\text{cm}^3$), $\lambda_{\text{ir.}} = 632.8 \text{ nm}$, $I = 0.0105 \text{ W}/\text{cm}^2$. (A) (1) without the dye; (2) for thickness of the stained layer $d = 500 \mu\text{m}$, $C(t)_{\text{rel}} = 0.715$, $t_{\text{stain}} = 10 \text{ min}$, $\mu_{\text{PS}} = 2.5 \text{ cm}^{-1}$; (B) (3) $C(t)_{\text{rel}} = 0.29$, $t_{\text{stain}} = 1.0 \text{ min}$, $\mu_{\text{PS}} = 4.64 \text{ cm}^{-1}$; (4) $C(t)_{\text{rel}} = 0.43$, $t_{\text{stain}} = 2.5 \text{ min}$, $\mu_{\text{PS}} = 6.91 \text{ cm}^{-1}$; (5) $C(t)_{\text{rel}} = 0.56$, $t_{\text{stain}} = 5.0 \text{ min}$, $\mu_{\text{PS}} = 8.96 \text{ cm}^{-1}$ 154
- Fig. 3-19 Temperature distribution over the cross section of the mucosal tissue layers: (A) (1) when irradiated with laser radiation at $\lambda_{\text{ir.}} = 670 \text{ nm}$, intensity $I = 0.09 \text{ W}/\text{cm}^2$ without the dye and (2) for thickness of the stained layer $d = 500 \mu\text{m}$, $C(t)_{\text{rel}} = 0.43$, $t_{\text{stain}} = 2.5 \text{ min}$, $\mu_{\text{PS}} = 25.9 \text{ cm}^{-1}$ (2); $C(t)_{\text{rel}} = 0.56$, $t_{\text{stain}} = 5 \text{ min}$, $\mu_{\text{PS}} = 34.0 \text{ cm}^{-1}$ (3); $C(t)_{\text{rel}} = 0.715$, $t_{\text{stain}} = 10 \text{ min}$, $\mu_{\text{PS}} = 43.0 \text{ cm}^{-1}$ (4); (B) (1) when irradiated with laser radiation at $\lambda_{\text{ir.}} = 632.8 \text{ nm}$, intensity $I = 0.0105 \text{ W}/\text{cm}^2$ without the dye and (2) for thickness of the stained layer $d = 500 \mu\text{m}$, $C(t)_{\text{rel}} = 0.29$, $t_{\text{stain}} = 1.0 \text{ min}$, $\mu_{\text{PS}} = 4.64 \text{ cm}^{-1}$; (3) $C(t)_{\text{rel}} = 0.43$, $t_{\text{stain}} = 2.5 \text{ min}$, $\mu_{\text{PS}} = 6.91 \text{ cm}^{-1}$; (4) $C(t)_{\text{rel}} = 0.56$, $t_{\text{stain}} = 5.0 \text{ min}$, $\mu_{\text{PS}} = 8.96 \text{ cm}^{-1}$ 155
- Fig. 3-20 Infrared absorption spectra of blood samples: before the magnetic therapy (1) and after one procedure (2) 158
- Fig. 3-21 Infrared absorption spectra of blood samples before (1) and after the magnetic therapy (2): for Amide I band (A), Amide III band (B). Deconvolution spectra of the corresponding bands before (3) and after the magnetic therapy (4) ($\Delta\nu_{1/2} = 30 \text{ cm}^{-1}$, $k_{\text{enh.}} = 2.5$) 159
- Fig. 3-22 Absorption spectra of blood samples in the range of $1000\text{--}1150 \text{ cm}^{-1}$: before (1) and after the magnetic therapy (2). Deconvolution spectrum of the blood sample after the magnetic therapy (3) ($\Delta\nu_{1/2} = 30 \text{ cm}^{-1}$, $k_{\text{enh.}} = 2.5$) 160
- Fig. 3-23 The ROS formation in the processes of single-electron reduction and excitation of oxygen 163

- Fig. 3-24 Changes of the oxygen partial pressure (Δp_{vO_2}) and arteriovenous oxygen difference (Δ_{AVD}) vs. photoinduced changes S_{vO_2} (ΔS_{vO_2}), obtained after the end of UVBI (●) and OVBI courses (□) ($\lambda_{ir} = 670$ nm). For Δp_{vO_2} vs. ΔS_{vO_2} : $r = 0.67$, $p < 0.001$ and for Δ_{AVD} vs. ΔS_{vO_2} : $r = -0.56$, $p < 0.001$ 169
- Fig. 3-25 Changes in the cholesterol concentration (ΔC_C) and APTT values (Δ_{APTT}) after the end of UVBI (●) and OVBI courses (□) ($\lambda_{ir} = 670$ nm) as functions of their initial values. For ΔC_C vs. C_C , $r = -0.67$, $p < 0.001$; for Δ_{APTT} vs. APTT – $r = -0.56$, $p < 0.001$ 170
- Fig. 4-1 The transmission spectra of the rat tissues: layers with thicknesses of 1 mm (1), 1.5 mm (2), and 2 mm (3) 188
- Fig. 4-2 The absorption spectra of the venous blood samples in rats (№ 3–5) in the range of 300–700 nm: (1) before OVBI and (2) after OVBI ($E = 7.5$ J/cm²) 190
- Fig. 4-3 The absorption spectra of venous blood samples in rats (№ 8–10) in the range of 650–1100 nm: (1) before irradiation; (2) after (laser+ γ) irradiation ($E = 7.5$ J/cm²); (3) after γ -irradiation (3Gy) 191
- Fig. 4-4 Infrared absorption spectra of the venous blood samples of rats: № 8.2 and № 10.2 after (laser+ γ) irradiation, № 8.3 and № 10.3 after γ -irradiation 192
- Fig. 4-5 Changes in the mean-group number of WBC and LYM under OVBI at $E = 7.5$ J/cm² and single γ -irradiation (3 Gy) in series of experiments (A) and (B), differing the mean-group initial cell number. WBC: (A) (1) control group, (2) single γ -irradiation; (3) 3 OVBI procedures followed by γ -irradiation; (B) (1) control group, (2) 3 OVBI procedures; (3) single γ -irradiation; (4) 3 OVBI procedures followed by γ -irradiation. LYM%: (A) (1) control, (2) γ -irradiation; (3) 3 OVBI procedures followed by γ -irradiation; (4) γ -irradiation followed by 3 OVBI procedures; (B) (1) control, (2) γ irradiation; (3) 3 OVBI procedures followed by γ -irradiation, (4) 3 OVBI procedures. (C) The relative changes in the mean-group number of C_{WBC} and C_{LYM} caused by γ -radiation (3 Gy) vs. initial concentrations ($C_{WBC}(C)$ and $C_{LYM}(C)$) 193
- Fig. 4-6 Changes in the mean-group RBC and Hb concentrations in series I with the most powerful changes. (A) RBC: (1) control group, (2) 3 OVBI procedures followed by γ -irradiation, (3) γ -irradiation (3 Gy), (4) γ -irradiation followed by 1 OVBI procedure ($E = 6.25$ J/cm²). Hb: (1) control group, (2) 3 preliminary OVBI procedures ($E = 7.5$ J/cm²), (3) γ -irradiation (3 Gy), (4) 3 OVBI procedures ($E = 7.5$ J/cm²) followed by γ -irradiation 196

- Fig. 4-7 Changes in PLT mean-group concentration at the laser energy density $E = 5 \text{ J/cm}^2$ and γ -radiation (3 Gy) in series of experiments (A) and (B), differing the mean-group initial values. (A): (1) control group; (2) γ -irradiation; (3) 4 OVBI procedures followed by γ -irradiation; (4) 4 OVBI procedures; (B): (1) control group; (2) γ - irradiation; (3) 4 OVBI procedures followed by γ -irradiation; (4) single γ -irradiation followed by 4 OVBI procedures; (5) 4 OVBI procedures. (C) The relative changes in the mean-group number of C_{PLT} caused by γ -radiation (3 Gy) as a function of the C_{PLT} initial concentration in peripheral blood of rats 198
- Fig. 4-8 Changes in the mean-group activity of SOD in blood samples of rats in two series of experiments (A) and (B), differing in the mean-group initial SOD activity. (A): (1) control group, (2) γ -irradiation (3Gy); (3) 3 OVBI procedures ($E = 7.5 \text{ J/cm}^2$) followed by γ -irradiation; B: (1) control group, (2) γ -irradiation; (3) 4 OVBI procedures ($E = 5 \text{ J/cm}^2$) followed by γ -irradiation; (4) preliminary γ -irradiation followed by 4 OVBI procedures ($E = 5 \text{ J/cm}^2$). C: The relative decrease in activity of SOD caused by γ -radiation as a function of the initial SOD activity ($C_{\text{SOD}}(C)$)..... 199
- Fig. 4-9 The relative number of cells: ($C_{\text{LIM}}(\text{laser} + \gamma)/C_{\text{LYM}}(\gamma)$) (●); $C_{\text{WBC}}(\text{laser} + \gamma)/C_{\text{WBC}}(\gamma)$ (□); $\text{LYM} \%(\text{laser} + \gamma)/\text{LYM} \%(\gamma)$ (▲)) vs. the relative values of the SOD activity obtained at the same conditions of combined and γ -irradiation 201
- Fig. 4-10 The changes in the individual number of leukocytes (ΔC_{WBC}) and lymphocytes (ΔC_{LYM}) as function of the initial values $C_{\text{WBC}}(C)$ or $C_{\text{LYM}}(C)$ in individual rats. (A): (1) γ -irradiation (3 Gy) (●); γ -irradiation and 3 followed OVBI procedures of at $E = 7.5 \text{ J/cm}^2$ (○); 4 OVBI procedures at $E = 5 \text{ J/cm}^2$ followed by γ -irradiation (▲) ($r = -0.5$, $p < 0.001$); (2) 4 OVBI procedures at $E = 5 \text{ J/cm}^2$ ($r = -0.85$, $p < 0.004$) (★); (B): γ -irradiation (3 Gy) (□); γ -irradiation followed by 3 OVBI procedures at $E = 18.75 \text{ J/cm}^2$ (▲); γ - irradiation followed by 3 OVBI procedures at $E = 7.5 \text{ J/cm}^2$ (●); ($r = -0.98$, $p < 0.001$)..... 203
- Fig. 4-11 Individual changes in ΔC_{Hb} and ΔC_{RBC} vs. initial values C_{Hb} and C_{RBC} in different rats. (A): γ -irradiation (3 Gy) (●); 3 preliminary OVBI procedures ($E = 7.5 \text{ J/cm}^2$) followed by γ -irradiation (■); 3 OVBI procedures ($E = 7.5 \text{ J/cm}^2$) (○); ($r = -0.68$, $p < 0.001$). (B): γ -irradiation (□); 3 OVBI procedures ($E = 7.5 \text{ J/cm}^2$) followed by γ -irradiation (●) 203
- Fig. 4-12 (A) Individual changes in C_{PLT} : ΔC_{PLT} vs. $C_{\text{PLT}}(C)$ ($E_{\text{OVBI}} = 5 \text{ J/cm}^2$) (1) γ -irradiation (■); γ -irradiation followed by 3 OVBI procedures at $C_{\text{PLT}}(C) = 944 \cdot 10^9/\text{L}$; ($r = -0.93$, $p < 0.001$) (●); (2) γ -

irradiation (\square), 4 OVBI procedures followed by γ -irradiation (\circ); γ -irradiation followed by 4 OVBI procedures (\triangle) at $C_{PLT}(C) = 708 \cdot 10^9/L$; ($r = -0.86$, $p < 0.002$). (B) Individual changes in SOD activity: 3 OVBI procedure ($E = 7.5 \text{ J/cm}^2$) followed by γ -irradiation (\bullet); γ -irradiation followed by 3 OVBI procedures ($E = 7.5 \text{ J/cm}^2$) (\triangle); 4 OVBI procedures ($E = 5 \text{ J/cm}^2$) followed by γ -irradiation (\square) ($r = -0.85$, $p < 0.0001$)..... 204

Fig. 4-13 The relative number of cells and SOD activity as a function of the total laser energy density E used at combined irradiation: several preliminary OVBI procedures followed by γ -irradiation (\bullet); preliminary γ -irradiation and then several OVBI procedures (\square) 206

LIST OF TABLES

Table 1-1 UVBI effect: on the maximum position of the plasma fluorescence spectra ($\lambda_{\max}^{\text{fl}}$) and their component ($\lambda_{\max}^{\text{fl}}$ (comp)); on the acid-based parameters (pH, $p_v\text{CO}_2$, HCO_3^-), measured on an ABL-800 instrument. The values of pH, $p\text{CO}_2$ and HCO_3^- are presented taking into account the coefficients of a variation for ABL-800 instrument.....	42
Table 2-1 Mean-group blood oxygenation values and the acid-based status of blood in CVD patients, the oxygen capacity of venous blood ct_vO_2 and arterial blood ct_aO_2 , the arteriovenous difference in the oxygen content AVDO_2 before the PT course and one day after the course, $p50$ —the partial pressure of O_2 at which $\text{S}_v\text{O}_2 = 50\%$	64
Table 3-1 Characteristics of the human tissues ($\lambda_{\text{ir.}} = 780\text{ nm}$)	140
Table 3-2 Characteristics of the human tissues ($\lambda_{\text{ir.}} = 670\text{ nm}$)	143
Table 3-3 Characteristics of the human tissues ($\lambda_{\text{ir.}} = 2000\text{ nm}$)	147
Table 3-4 Optical and thermal characteristics of mucosal tissue.....	153
Table 4-I Relative changes ($\gamma/\text{control}$) in the mean-group RBC and Hb concentrations, Hct values in various series of experiments.....	195
Table 4-2 Radioprotective effect of laser radiation on the main parameters of peripheral blood and the activity of antioxidant enzymes under γ -irradiation of the whole body of rats (3 Gy) and different variants of OVBI.....	200

ACKNOWLEDGEMENTS

We are very grateful to our colleague-scientists, whose help made a contribution to the writing of this monograph:

Professor Ulastchik V.S.–Academician of the National Academy of Sciences of Belarus, Professor, D. Sc. (Med), a scientific editor of the first edition of this monograph in 2014; many thanks for valuable advices and comments;

Professors, D. Sc. (Med.): Nechipurenko N.I., Kirkovski V.V., Marochkov A.V. – Competent consultants on the use of UV and intravenous blood irradiation in medical practice;

Professors, D. Sc. (Phys. & Math.): Asimov M.M, Zeltov G.I., Bushuk B.A., Dzagarov B.M., many thanks for fruitful discussion of photophysical processes initiated by low-intensity optical radiation in human tissues;

Sambor E.G., Kuchinskii A. V., Maslova T.O., Galay O.A., Karoza A.V., Batay L.E.–Colleagues from the B.I. Stepanov Institute of the Physics of the National Academy of Sciences of Belarus, conducted experiments and Astaf'eva L.G. for invaluable assistance in modeling the optical radiation propagation in human tissues; special thanks to Kalosha I.I. for both many-year fruitful cooperation and invaluable help in discussing and preparing the monograph;

Laskina O.V. – Assistant of the 3rd Department of Internal Medicine at the Belarussian State Medical University; whose enthusiasm and dedicated work arrived at the unique results on the individual sensitivity of patients to low-intensity optical radiation effects;

Nasek V.M., Zilberman R.G. – Colleagues from the Institute of Bioorganic Chemistry of the National Academy of Sciences of Belarus and Koshlan I.V. – Colleague from the Joint Institute for Nuclear Research (Dubna, Russia) for assistance in conducting experiments on the combined effects of gamma and laser irradiations on rats.

We are very much obliged for your help.

INTRODUCTION

The optical radiation effect on blood in blood vessels and tissues, used for therapeutic purposes, is one of the methods of a phototherapy (PT) that is the fastest-growing field of modern medicine. Laser medicine originated in the second half of the twentieth century; it should be viewed as a PT subset that is one of the oldest therapeutic methods. PT was initially utilized in medical practice as solar therapy, then light therapy, and then as ultraviolet blood irradiation that has been in use in medicine for 70 years. Currently, PT performed as intravenous and overvein blood irradiation with low-intensity optical radiation is considered as a method of biostimulation suitable for treating a wide range of diseases. Evidence has emerged that the combined effects of phototherapy and drug treatment improve treatment outcomes.

So far, the expansion of the scope of applications of intravenous and overvein blood irradiation has been empirical. The widespread use of these methods in medical practice was limited by a lack of generally accepted ideas about the primary molecular mechanism of the optical radiation action on blood irradiated *in vivo*. The previously proposed biostimulation mechanisms, based on the analysis of various secondary reaction products, obtained by irradiating cell cultures and biotissues, remained at the level of the hypotheses unable to explain many experimental facts. In addition, it was impossible to predict the PT effects on a living organism by the processes detected in cell cultures and in isolated tissues. It appeared that a direct comparison of the effects observed in model experiments and in a living organism poses great difficulties. The same PT methods, with identical energy densities of light exposure, initiated improvements in some patients and unpredictable negative reactions in others. The positive and negative treatment results were not explained scientifically. Such topical photobiostimulation problems remained unresolved, as the development of methods for assessing their effectiveness for individual patients and the creation of methods for standardization and control.

In this regard, the study of photoreactions initiated in blood by therapeutic doses of the optical radiation at different wavelengths, the determination of laws of blood photomodification, and the identification of factors that most affect the individual patient sensitivity to the blood irradiation are among the urgent tasks of PT. Solving these problems will

contribute to deepening our understanding of PT mechanisms and also further expand the applications of laser-optical technologies in medicine.

ABOUT THE STRUCTURE OF THE BOOK

The book is founded on the experimental results of the authors. The main purpose of this book is to propose and substantiate PT molecular mechanisms with the implication of photophysical processes initiated by low-intensity optical radiation. The book is organized in four chapters, a conclusion and a bibliography.

According to the basic law of photochemistry, a photochemical reaction in blood can occur only if irradiated blood is capable of absorbing incident light. In Chapter One, we studied the spectral characteristics of whole blood, red cells and plasma before and after UV extracorporeal, intravenous and overvein blood irradiation by low-intensity laser-optical radiation at different wavelengths. The spectral manifestations of photochemical processes initiated in blood under PT were explored and explained in order to examine the irradiation effects at the molecular level. Fluorescent spectroscopy was adopted to investigate possible structural changes in plasma macromolecules after the blood irradiation *in vivo*.

In Chapter Two, the research objects were blood gas composition, a degree of hemoglobin oxygen saturation in venous and arterial blood, acid-based balance indices, erythrocyte and hemoglobin concentrations, as well as contents of some metabolic products under PT. A study of changes initiated by PT in the partial pressure of blood gases and in the degree of hemoglobin oxygen saturation is a further step in identifying the photoacceptor molecule. Based on these data, the blood irradiation effect on the oxygen status of venous and arterial blood, the oxygen supply to the organs and tissues, and the oxygen utilization was studied. The blood oxygenation dynamics during the PT courses was defined as well. The changes in hematocrit, hemoglobin concentration, and erythrocyte count at low-intensity optical radiation doses were monitored during the PT course. Special attention was given to the susceptibility of individual patients to blood irradiation, and methods for its control were suggested.

A significant part of this chapter was devoted to metabolic processes under PT. Using glucose and lactate (playing an important role in metabolic processes), as an example we studied the PT effect on their concentrations. We showed that therapeutic doses of the optical radiation absorbed by blood cause short- and long-term changes in lactate and glucose concentrations in blood of patients. The dependences of

concentration changes initiated by PT on both the initial concentrations and the photoinduced variations in the blood oxygenation were analyzed.

Using the optical radiation of various wavelengths, we investigated the PT effects on blood coagulation parameters in different patients. The concentration changes in total cholesterol, triglycerides, low-density lipoprotein cholesterol, and high-density lipoprotein cholesterol were estimated. A relationship between the photoinduced changes in blood oxygenation characteristics and the concentrations of metabolic products was analyzed. Possible molecular mechanisms were considered for the effects observed.

Chapter Three was devoted to analyzing the molecular mechanism of the PT action. First, a brief review based on the analysis of literature data was presented. It covered the proposed mechanisms of therapeutic action of laser-optical radiation. It should be noted that before our studies, the PT effect on a living organism had not been sufficiently analyzed at the molecular level.

The hypothesis that local heating of blood or tissues in the absorption zone is a starting mechanism for biostimulation has been actively discussed to date. We therefore performed a computer simulation of thermal fields and estimated heating temperatures at the tissue surface, in tissues, and in venous blood at low- and high-intensity laser irradiation. Computer modeling of low-intensity optical radiation effects in mucosal tissues was used to explore the mechanism of the optical radiation action on tissues stained by photosensitizers.

The choice of a wavelength for PT is another medical problem, for the solution of which the optical properties of blood and tissues are extremely important. The optical properties of blood and human tissues were briefly summarized. Based on these data, spectra of the radiation penetration depth into blood and skin tissues were calculated in the wavelength range of 405–950 nm. The wavelengths optimal for PT were then determined. Molecular oxygen is effectively formed during intravenous and overvein blood irradiation with the optical radiation at these wavelengths.

Based on the results obtained, we proposed a molecular mechanism for the therapeutic action capable of explaining a number of effects that had not been interpreted unambiguously for many years. The main photoactivation stages of the organism were suggested. The possible role of reactive oxygen species in the therapeutic action of low-intensity optical radiation was considered. The applicability of the proposed PT mechanism was discussed to explain the therapeutic effects observed in treating a wide range of diseases.

In Chapter Four, which deals with rat experiments, the radioprotective possibilities of low-intensity optical radiation were used to study the actual problem of counteracting the destructive action of ionizing radiation. The available literature data have no convincing confirmation of the radioprotective capability of low-intensity optical radiation. The effect of *in vivo* blood irradiation with the laser radiation on the hematological parameters and the antioxidant protection enzymes for gamma-exposed rats was examined. The quantitative changes caused by low-intensity laser radiation and gamma radiation in blood cells were analyzed. Differences in the individual radiosensitivity of rats were investigated. The molecular mechanisms of the radioprotective effect of low-intensity optical radiation, as well as the factors affecting the individual sensitivity of rats were discussed.

In conclusion, the results obtained by the authors of the book were summarized. The most important results were emphasized. In our opinion, they will contribute to a further successful use of PT in medical practice. Some important issues, which remained unresolved despite a rapid growth of a number of PT studies, were considered. Further research areas are outlined.

The book summarizes the interdisciplinary research results, and will be of interest to researchers in photophysics, biophysics, physiotherapy, as well as to physicians using phototherapy in complex treatment and rehabilitation of patients. The book is also intended as a teaching tool either for graduate students or students interested in physical medicine problems.

ABBREVIATIONS

ACS	–	Acute coronary syndrome
AOS	–	Antioxidant system
aPPT	–	Activated partially prothromboplastin time
AVDO ₂	–	Arteriovenous oxygen difference
Ca ²⁺	–	Calcium ions
CO ₂	–	Carbon dioxide
ConO ₂	–	Consumption of oxygen
CVD	–	Cardiovascular disease
CAT	–	Catalase
C _{util}	–	Coefficient of oxygen utilization
ct _a O ₂	–	Oxygen capacity in arterial blood
ct _v O ₂	–	Oxygen capacity in venous blood
DRA	–	Deoxyribonucleic acid
2,3-DFG	–	2,3-Diphosphoglycerate
DO ₂	–	Delivery of oxygen
EFME	–	Electrophoretic mobility of erythrocyte
EMT	–	Extracorporeal magnetotherapy
F _v (HbO ₂)	–	Content of oxyhemoglobin fraction
GRA	–	Granulocyte
Gy	–	Gray
Hct	–	Hematocrit
Hb	–	Hemoglobin
H ⁺	–	Hydrogen ions
H ₂ O ₂	–	Hydrogen peroxide
HbO ₂	–	Oxyhemoglobin
HCO ₃ [–]	–	Hydrocarbonate ion
IR	–	Ionizing radiation
INR	–	International normalized ratio
IVBI	–	Intravenous blood irradiation
k _{enh}	–	Resolution enhancement factor
KRS	–	Thallium bromide iodide mixed crystal
LED	–	Light emitting diode
LILR	–	Low intensity laser radiation
LIOR	–	Low intensity optical radiation

LPO	–	Lipid peroxidation
LYM	–	Lymphocyte
MCV	–	Mean erythrocyte volume
MetHb	–	Methemoglobin
MF	–	Magnetic field
MT	–	Magnetic therapy
NO	–	Nitrogen oxide
ODC	–	oxyhemoglobin dissociation curve
OTFB	–	Oxygen transport function of blood
OVBI	–	Overvein blood irradiation
O ₂		Oxygen
¹ O ₂	–	Singlet oxygen
O ₂ [–]	–	Superoxide anion radical
PMM	–	Primary molecular mechanism
PPA	–	Primary photoacceptor
pH	–	Blood acidity
P ₅₀	–	Oxygen partial pressure at which hemoglobin is 50% saturated
Δp _v O ₂	–	Oxygen partial pressure in venous blood
p _v CO ₂	–	Carbon dioxide partial pressure in venous blood
r	–	Pearson linear correlation coefficient
RBC	–	Erythrocyte
RNA	–	Ribonucleic acid
ROS	–	Reactive oxygen species
SOD	–	Superoxide dismutase
TCT	–	Trombin clotting time
UV	–	Ultraviolet
UVBI	–	Ultraviolet blood irradiation
S _v O ₂	–	Hemoglobin oxygen saturation in venous blood
V _{er}	–	Volume of red blood cell
WBC	–	Leukocyte
γ	–	Gamma radiation
η _{bl}	–	Blood viscosity
η _{pl}	–	Plasma viscosity
λ	–	Wavelength
Δν _{1/2}	–	Half width of absorption band

CHAPTER ONE

THE EFFECT OF LOW-INTENSITY OPTICAL RADIATION ON THE SPECTRAL-LUMINESCENT CHARACTERISTICS OF BLOOD IRRADIATED *IN VIVO*

1.1 Electronic absorption spectra of whole blood, erythrocytes and plasma

Absorption spectroscopy is widely used to study the physicochemical properties of biological objects [1–3]. The position of absorption bands, and their half-width and intensity provide information on a qualitative and quantitative ratio of the components of biological systems and on their structural organization in the ground electronic state.

In the wavelength range of 210–250 nm, a number of blood components are absorbed: residues of aliphatic amino acids of proteins, free aliphatic amino acids of blood plasma, lipids of a membrane and plasma, polysaccharides, and some other non-protein organic components of blood plasma. In the range of 250–300 nm, the absorption occurs due to residues of aromatic amino acids: tryptophan, tyrosine, and phenylalanine. Of these, tryptophan has the highest absorption coefficient at a wavelength of 254 nm which is used in UV devices for the blood irradiation. Free amino acids and radicals of blood plasma that play an important role in initiating photooxidation reactions of unsaturated fatty acids are also absorbed within this range. It should be noted that UV radiation at 254 nm used for therapeutic purposes is photochemically active and can cause a breakdown of nucleic acids, proteins and lipids.

The absorption spectra of whole blood, erythrocytes and plasma are shown in Fig. 1-1. The shortwave absorption band, with a maximum wavelength of $\lambda_{\text{max}} = 280$ nm, is present in the spectra of all proteins containing aromatic amino acid residues.

The absorption bands of deoxyhemoglobin at $\lambda_{\text{max}} = 430$ and 555 nm, as well as the oxyhemoglobin bands at $\lambda_{\text{max}} = 344, 415, 541$ and 577 nm,

which appear in the blood and erythrocyte spectra, are caused by the absorption of iron porphyrin being part of hemoglobin [4]. Hemoglobin is a protein globule-tetramer. It is formed by four polypeptide chains, each of which is an individual molecule containing a protoporphyrin chelate complex with iron (heme), capable of attaching ligands (O_2 , CO , NO , etc.). In the UV range, the absorption bands at $\lambda_{\max}=274$ nm for deoxyhemoglobin and $\lambda_{\max}=276$ nm for oxyhemoglobin, corresponding to their shortest wave transition, are masked by the absorption of proteins.

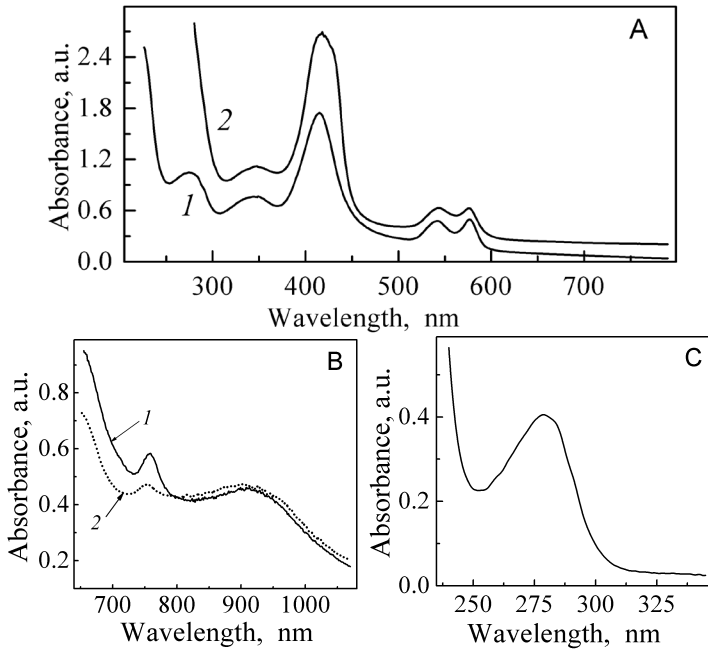


Fig. 1-1 Absorption spectra: whole blood (A1) and erythrocytes (A2), whole blood with a higher concentration of oxyhemoglobin (B2) and with a lower one (B1); plasma (C)

In the absorption spectrum of all hemoglobins, the most intense among iron-porphyrin bands is the Soret band ($k=140 \text{ mM}^{-1}\cdot\text{cm}^{-1}$), the maximum of which can be between $410 < \lambda_{\max} < 430$ nm. According to the data [5], in the range of the Soret band, the electronic absorption spectra of porphyrins have two resolved high-intensity bands which belong to transitions, polarized mutually perpendicularly. High-frequency asymmetry of the band contour is due to the vibrational structure. The assignment of the